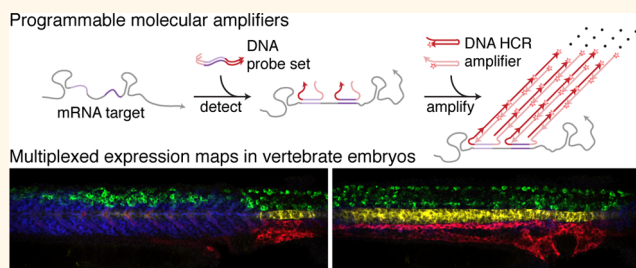


Next-Generation *in Situ* Hybridization Chain Reaction: Higher Gain, Lower Cost, Greater Durability

Harry M. T. Choi,[†] Victor A. Beck,[†] and Niles A. Pierce^{†,‡,*}

[†]Division of Biology & Biological Engineering and [‡]Division of Engineering & Applied Science, California Institute of Technology, Pasadena, California 91125, United States

ABSTRACT Hybridization chain reaction (HCR) provides multiplexed, isothermal, enzyme-free, molecular signal amplification in diverse settings. Within intact vertebrate embryos, where signal-to-background is at a premium, HCR *in situ* amplification enables simultaneous mapping of multiple target mRNAs, addressing a long-standing challenge in the biological sciences. With this approach, RNA probes complementary to mRNA targets trigger chain reactions in which metastable fluorophore-labeled RNA hairpins self-assemble into tethered fluorescent amplification polymers. The properties of HCR lead to straightforward multiplexing, deep sample penetration, high signal-to-background, and sharp subcellular signal localization within fixed whole-mount zebrafish embryos, a standard model system for the study of vertebrate development. However, RNA reagents are expensive and vulnerable to enzymatic degradation. Moreover, the stringent hybridization conditions used to destabilize nonspecific hairpin binding also reduce the energetic driving force for HCR polymerization, creating a trade-off between minimization of background and maximization of signal. Here, we eliminate this trade-off by demonstrating that low background levels can be achieved using permissive *in situ* amplification conditions (0% formamide, room temperature) and engineer next-generation DNA HCR amplifiers that maximize the free energy benefit per polymerization step while preserving the kinetic trapping property that underlies conditional polymerization, dramatically increasing signal gain, reducing reagent cost, and improving reagent durability.



KEYWORDS: dynamic nucleic acid nanotechnology · programmable molecular instruments · conditional self-assembly · fluorescence *in situ* hybridization

Life is orchestrated by programmable biomolecules interacting within complex biological circuits. One of the central technical challenges in biological research is the difficulty in interrogating the state of these circuits within intact organisms. In this pursuit, *in situ* hybridization methods provide biologists with a powerful tool for mapping mRNA expression in a morphological context. However, with traditional approaches, it remains challenging to simultaneously map the expression patterns of multiple target mRNAs within a single intact vertebrate embryo, hindering the study of development and disease in model systems most relevant to human biology.

With *in situ* hybridization, nucleic acid probes are used to detect complementary nucleic acid targets within fixed samples; subsequent washes remove unbound probes prior to imaging of fluorophores or chromophores that either label the probes

directly or are localized in the vicinity of probes during a subsequent amplification step.^{1,2} Direct-labeled fluorescent probes are well suited for multiplexing,^{3–9} but do not generate sufficient signal-to-background for general-purpose use within intact vertebrate embryos. To improve the signal-to-background ratio, significant effort has been devoted to the development of *in situ* amplification methods.^{6,10–21} In the demanding imaging environment of whole-mount vertebrate embryos, traditional approaches employ enzymes to catalyze the deposition of reporter molecules in the vicinity of nucleic acid probes.^{22–25} These methods are widely used despite significant drawbacks. Spatial resolution is typically compromised by diffusion of reporter molecules prior to deposition,^{26,27} and the lack of orthogonal deposition chemistries dictates that *in situ* amplification be performed serially for multiplexed studies,^{24,25,28,29} leading to progressive sample degradation

* Address correspondence to
niles@caltech.edu.

Received for review November 4, 2013
and accepted March 31, 2014.

Published online
10.1021/nn405717p

© XXXX American Chemical Society

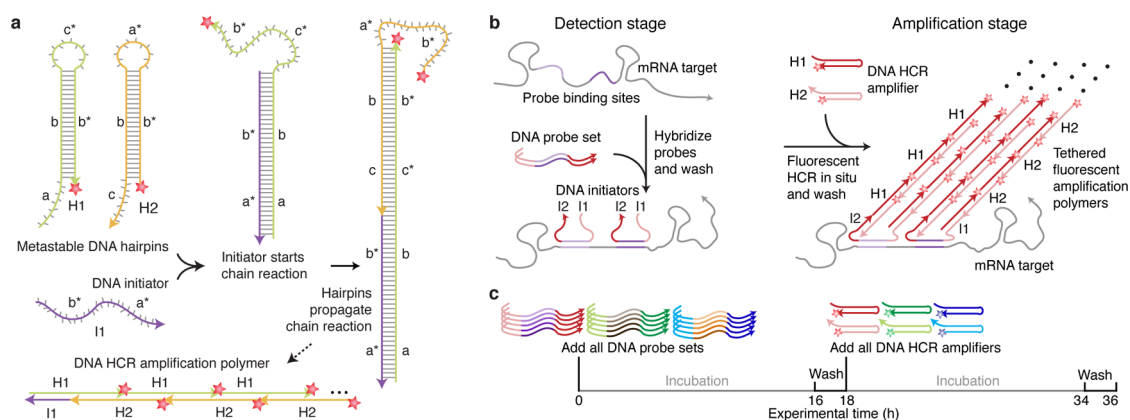


Figure 1. *In situ* amplification via hybridization chain reaction (HCR). (a) HCR mechanism. Metastable fluorescent hairpins self-assemble into fluorescent amplification polymers upon detection of a cognate initiator. Initiator I1 nucleates with hairpin H1 via base-pairing to single-stranded toehold "a", mediating a branch migration^{69,70} that opens the hairpin to form complex I1·H1 containing single-stranded segment "c*-b*". This complex nucleates with hairpin H2 by means of base-pairing to toehold "c", mediating a branch migration that opens the hairpin to form complex I1·H1·H2 containing single-stranded segment "b*-a*". Thus, the initiator sequence is regenerated, providing the basis for a chain reaction of alternating H1 and H2 polymerization steps. Red stars denote fluorophores. (b) *In situ* hybridization protocol. Detection stage: probe sets are hybridized to mRNA targets, and unused probes are washed from the sample. Amplification stage: initiators trigger self-assembly of tethered fluorescent amplification polymers, and unused hairpins are washed from the sample. (c) Experimental timeline. The same two-stage protocol is used independent of the number of target mRNAs. For multiplexed experiments (three-color example depicted), probe sets for different target mRNAs (five probes depicted per set) carry orthogonal initiators that trigger orthogonal HCR amplification cascades labeled by spectrally distinct fluorophores.

and lengthy protocols. For example, it takes 5 days to map three target mRNAs in succession in a whole-mount chick embryo.^{24,29} Drawing on principles from the emerging discipline of dynamic nucleic acid nanotechnology,³⁰ we previously overcame this four-decade-old challenge³¹ by engineering orthogonal molecular amplifiers based on the mechanism of hybridization chain reaction (HCR),³² enabling parallel *in situ* amplification for up to five target mRNAs within whole-mount zebrafish embryos.³³

An HCR amplifier consists of two kinetically trapped nucleic acid hairpin molecules (H1 and H2) that coexist metastably in the absence of a cognate initiator strand (I1; Figure 1a). Arrival of the initiator triggers a chain reaction in which H1 and H2 hairpins sequentially nucleate and open to assemble into a long nicked double-stranded amplification polymer.³² HCR signal amplification has been exploited for diverse technological purposes *in vitro* and *in situ*. By integrating HCR initiators into a variety of molecular probes, including hybridization-based nucleic acid probes,^{33–41} aptamers,^{32,36,42–47} antibodies,^{42,48–55} functionalized nanoparticles,^{45,49–51,53–55} and DNazymes,⁵⁶ HCR amplification has been applied to the detection of diverse classes of targets, including nucleic acids,^{32–35,37–41,46,57–68} proteins,^{36,42–53,55} and small molecules.^{32,54,56} HCR amplification cascades have been used to generate diverse output signals, including fluorescence,^{33,42–44,48,51,57–61,63,64,66,67} chemiluminescence,^{34,39,52} bioluminescence,⁴⁶ color,^{34,62,63,68} electrochemical impedance,^{36,38,40,41,45,47,49,50,53–56} electrochemical chemiluminescence,³⁷ and energy dissipation.^{35,65}

Several conceptual properties of HCR are particularly well suited to the challenges of *in situ* amplification. First,

HCR is programmable, providing a basis for straightforward multiplexing using amplifiers that recognize different initiator sequences and operate independently. Second, HCR self-assembly is conditional on the presence of the initiator, enabling hairpins to penetrate the sample prior to assembling into long amplification polymers *in situ*. Third, HCR amplification polymers are expected to remain tethered to their initiators, preventing diffusion of the amplified signal away from the target site.

Consistent with these properties, HCR *in situ* amplification enabled straightforward multiplexing in whole-mount zebrafish embryos, achieving deep sample penetration, high signal-to-background, and sharp signal localization.³³ Crucially, the same two-stage protocol was used independent of the number of target mRNAs (Figure 1bc). In the detection stage, all probes were introduced in parallel, and unused probes were washed from the sample. In the amplification stage, all HCR amplifiers were introduced in parallel, and unused hairpins were washed from the sample.

Having completed development and validation of the first-generation HCR *in situ* amplification technology,³³ we set out to improve reagent performance, cost, and durability by revisiting key engineering challenges and decisions. The motivation for using *in situ* amplification is the difficulty in achieving high signal-to-background when mapping mRNA expression within intact vertebrate embryos. Background arises from three sources: autofluorescence (inherent fluorescence of the fixed sample), nonspecific detection (probes that bind nonspecifically and are subsequently amplified), and nonspecific amplification (HCR hairpins that bind

nonspecifically within the sample). To destabilize nonspecific binding, *in situ* hybridization experiments are typically performed in stringent hybridization conditions. In the context of HCR *in situ* amplification, we previously found this strategy to be essential and successful: in permissive conditions, HCR hairpins bound nonspecifically in the sample;⁷¹ in stringent conditions, nonspecific hairpin binding was negligible.³³ However, performing HCR *in situ* amplification in stringent conditions has an important drawback: destabilizing nonspecific binding simultaneously reduces the energetic driving force for HCR polymerization, reducing the number of hairpins per HCR polymer and, hence, amplifier gain. Indeed, in stringent hybridization conditions, DNA HCR amplifiers engineered to operate in permissive conditions³² produced no detectible signal *in situ*.⁷¹ We overcame this difficulty using two complementary approaches, both of which increased the cost of the first-generation technology.³³ First, to partially counteract base-pair destabilization in stringent hybridization conditions, we switched from DNA probes and HCR hairpins to RNA probes and HCR hairpins in order to exploit the enhanced stability of RNA hybridization. Second, we detected each target mRNA using a probe set containing multiple probes^{4,9} each carrying the same initiator, yielding multiple tethered amplification polymers per target. For example, to map the expression of five target mRNAs in whole-mount zebrafish embryos, we employed probe sets containing between 7 and 30 probes per target.³³ Unfortunately, RNA oligo synthesis is substantially more expensive than DNA oligo synthesis and, moreover, the cost per probe set increases linearly with the number of probes. Additionally, RNA reagents are vulnerable to enzymatic degradation and require careful handling on the benchtop.

In the present work, we set out to engineer better solutions to these challenges. To decrease reagent cost and improve reagent durability, we set the hard constraint that RNA probes and amplifiers be replaced by new DNA probes and amplifiers engineered to be suitable for use *in situ*. To increase the signal gain per amplifier, we set out to increase the energetic driving force for HCR polymerization *via* two complementary approaches: first, by establishing permissive *in situ* amplification conditions that avoid the expected increase in nonspecific reagent binding; second, by engineering DNA HCR hairpins that maximize the free energy benefit per polymerization step while preserving the kinetic trapping property that underlies conditional polymerization. These engineering efforts yielded a next-generation DNA HCR *in situ* amplification technology that dramatically improves on the performance, cost, and durability of the first-generation RNA technology, providing biologists with superior programmable molecular instruments for mapping the state of endogenous biological circuitry within intact organisms.

RESULTS AND DISCUSSION

Permissive Hybridization Conditions for DNA HCR *in Situ* Amplification. We began by seeking to determine whether, contrary to standard practice^{1,2} and our own experience,^{33,71} it might be possible to identify permissive hybridization conditions that do not cause high background due to nonspecific binding of nucleic acid reagents within whole-mount vertebrate embryos. To our surprise, we were able to identify permissive hybridization conditions (0% formamide, room temperature) that cause minimal nonspecific binding of DNA hairpins in whole-mount zebrafish embryos (Section S2 in the SI), affording us the opportunity to engineer next-generation DNA HCR amplifiers for use in hybridization conditions conducive to the growth of high-gain HCR polymers.

Engineering High-Gain DNA HCR Amplifiers for Use in Permissive Hybridization Conditions. Having identified permissive *in situ* amplification conditions, we set out to engineer DNA HCR hairpins that maximize the free energy benefit per polymerization step while retaining hairpin metastability in these conditions. The free energy benefit per polymerization step increases with loop/toehold length and is independent of stem length (stem base pairs are present in both the hairpins and the polymer). By contrast, empirical evidence suggests that hairpin metastability decreases with loop/toehold length and increases with stem length. On the basis of these properties, we exploited the following HCR design rules to dimension hairpins for use in a given set of experimental conditions:

- Increase the loop/toehold length until H1 and H2 hairpins begin to form putative heterodimers. Fix the loop/toehold length just below this threshold to maximize the free energy benefit per polymerization step.
- Increase the stem length until the hairpins coexist metastably in the absence of the initiator.

Using these design rules for DNA hairpins in 5× SSCT buffer at 25 °C, we arrived at 12-nt toeholds/loops and 24-bp stems.

Previously, to achieve HCR amplification in stringent hybridization conditions, we engineered RNA HCR hairpins with 10-nt toeholds/loops and 16-bp stems.³³ Figure 2 compares the test tube performance of the first-generation RNA HCR hairpins in stringent conditions (40% formamide, 45 °C) to that of the new DNA HCR hairpins in permissive conditions (0% formamide, room temperature). For the RNA system, the hairpins are predominantly metastable after 1.5 h, but have predominantly leaked out of their kinetic traps to form uninitiated polymers overnight (Figure 2a). For the DNA system, the hairpins are predominantly metastable even after an overnight reaction (Figure 2b). As the initiator concentration decreases, the mean DNA polymer length is substantially longer than the

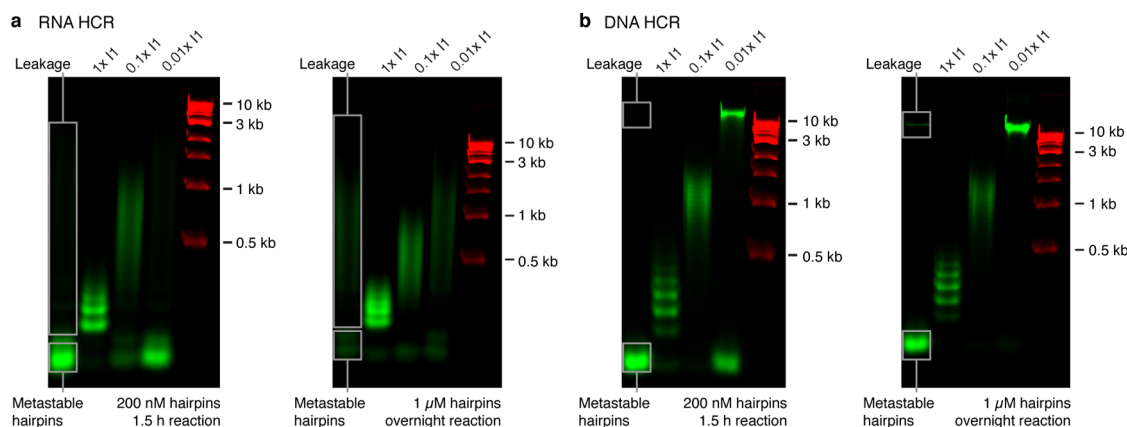


Figure 2. Comparing *in vitro* amplification performance for (a) published RNA HCR³³ in stringent amplification conditions (40% formamide, 45 °C) and (b) next-generation DNA HCR in permissive amplification conditions (0% formamide, room temperature). For each system, reactions were run with 200 nM of each hairpin for 1.5 h (to challenge polymer growth) and with 1 μ M of each hairpin overnight (to challenge hairpin metastability). Agarose gels demonstrating hairpin metastability in the absence of initiator and increasing polymer length with decreasing initiator concentration (1 \times , 0.1 \times , 0.01 \times I1). Green channel: HCR-Alexa647. Red channel: dsDNA ladder prestained with SYBR Gold.

mean RNA polymer length. Hence, the DNA hairpins in permissive amplification conditions exhibit superior metastability and generate higher signal gain than the RNA hairpins in stringent amplification conditions.

Multiplexed Signal Amplification Using Orthogonal DNA HCR Amplifiers. Because HCR function relies on the programmable chemistry of nucleic acid base-pairing, it is straightforward to program multiple amplifiers that operate independently and are hence suitable for parallel multiplexing *in vitro* or *in situ*. After establishing the dimensions of the new DNA HCR hairpins, we designed multiple amplifiers using the multistate sequence design feature of the NUPACK web application.⁷² Sequences were optimized for a set of target secondary structures representing key initial and intermediate states in the polymerization cascade, with the goal of reducing the ensemble defect for each target structure below a user-specified stop condition.⁷³ For a given target secondary structure and candidate sequence, the ensemble defect is the average number of incorrectly paired nucleotides at equilibrium evaluated over the ensemble of unspseudoknotted secondary structures.^{73,74}

For a set of DNA HCR amplifier designs, equilibrium test tube calculations^{72,75} were used to step through the intended molecular assembly operations to verify that the initiators, hairpins, and polymerization intermediates are predicted to be well formed with high yield (sometimes with weak secondary structure in toeholds or loops that are intended to be unstructured) and that each amplifier is predicted to be orthogonal to the initiators of the other amplifiers (Section S3 in the SI). The multiplexed *in vitro* validation study of Figure 3 demonstrates four of these DNA HCR amplifiers operating simultaneously and orthogonally in permissive hybridization conditions. The hairpins exhibit metastability in the absence of initiators, and each initiator selectively triggers the cognate polymerization cascade.

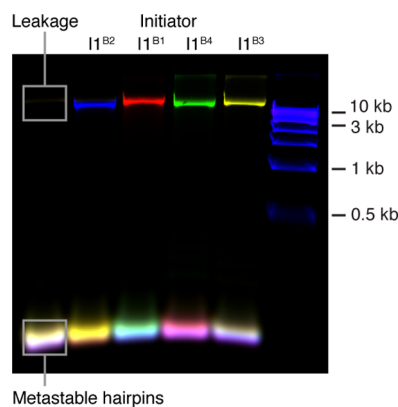


Figure 3. Multiplexed signal amplification using four orthogonal DNA HCR amplifiers (B1, B2, B3, B4). Agarose gel demonstrating minimal leakage in the absence of initiators and strong activation of the cognate amplifier by each of four initiators (I1^{B1}, I1^{B2}, I1^{B3}, I1^{B4}). Reaction conditions: 4 HCR amplifiers in all reactions, 400 nM for each hairpin, 0.01 \times initiator, 5 \times SSCT buffer, 4 h reaction at room temperature. See Section S3 in the SI for additional data.

Comparing RNA HCR and DNA HCR *In Situ* Amplification. Using confocal microscopy, Figure 4 compares the *in situ* performance of RNA HCR in stringent amplification conditions³³ and DNA HCR in permissive amplification conditions for a highly expressed transgenic target in whole-mount zebrafish embryos. Each method uses only a single 50-nt probe of the corresponding material carrying a single HCR initiator. With the microscope gain adjusted to avoid saturating pixels in the DNA HCR image, the signal in the RNA HCR image is nearly undetectable to the human eye (Figure 4a). Histograms of pixel intensities show that the overlap between the distribution of total fluorescence (signal + background) and the distribution of background is already small with the RNA method and becomes negligible with the DNA method (Figure 4b). The mean signal increases \sim 5-fold using DNA vs RNA

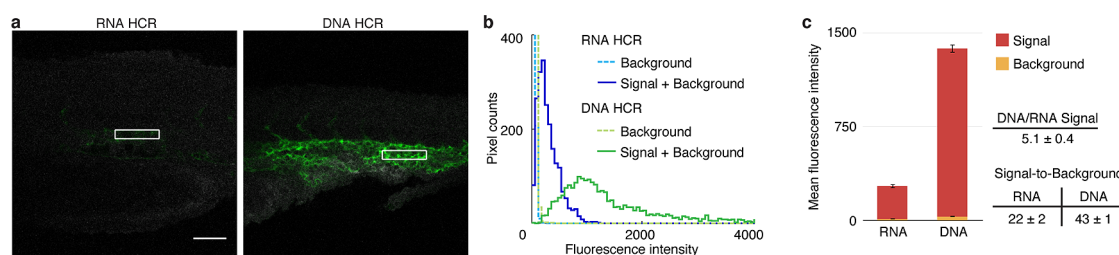


Figure 4. Comparing *in situ* amplification performance for published RNA HCR³³ in stringent amplification conditions (40% formamide, 45 °C) and next-generation DNA HCR in permissive amplification conditions (0% formamide, room temperature). (a) mRNA expression imaged by confocal microscopy with the microscope gain adjusted to avoid saturating pixels using DNA HCR. Sample: whole-mount zebrafish embryo. Target: transgenic mRNA *Tg(flk1:egfp)*. Probe sets: one RNA or DNA probe. Green channel (excitation 633 nm): HCR-Alexa647 staining plus autofluorescence. Gray channel (excitation 488 nm): autofluorescence to depict sample morphology. Embryos fixed: 27 hpf. Scale bar: 50 μ m. (b) Pixel intensity histograms for background (in WT embryos lacking the target; depicted rectangles in Figures S13 and S14 in the SI) and signal plus background (in transgenic embryos containing the target; depicted rectangles in panel (a)). (c) Characterizing signal and background contributions for representative rectangles (mean \pm standard deviation, $N = 3$ embryos). See Section S4.1 in the SI for additional data.

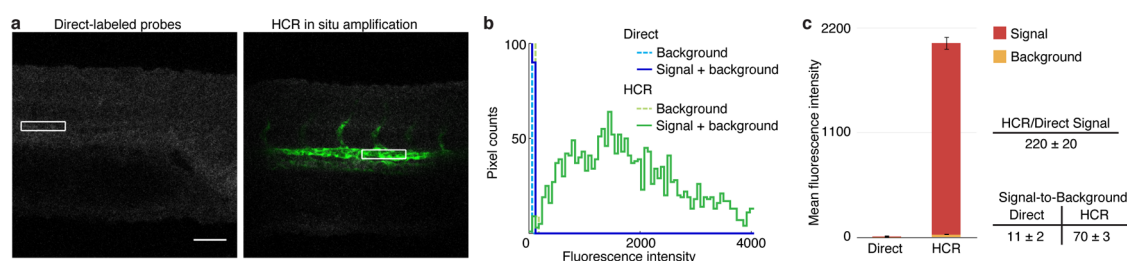


Figure 5. Comparing signal strength using direct-labeled DNA probes without and with DNA HCR *in situ* amplification. (a) mRNA expression imaged by confocal microscopy with the microscope gain adjusted to avoid saturating pixels using DNA HCR. Sample: whole-mount zebrafish embryo. Target: transgenic mRNA *Tg(flk1:egfp)*. Probe set: five Alexa647-labeled one-initiator DNA probes. Green channel (excitation 633 nm): probe-Alexa647 staining plus autofluorescence without or with HCR-Alexa647 staining. Gray channel (excitation 488 nm): autofluorescence to depict sample morphology. Embryos fixed: 27 hpf. Scale bar: 50 μ m. (b) Pixel intensity histograms for background (in WT embryos lacking the target; depicted rectangles in Figure S17 in the SI) and signal plus background (in transgenic embryos containing the target; depicted rectangles in panel (a)). (c) Characterizing signal and background contributions for representative rectangles (mean \pm standard deviation, $N = 3$ embryos). See Section S4.2 in the SI for additional data.

HCR, consistent with the growth of longer HCR amplification polymers *in situ*. The mean background intensity increases ~ 2.5 -fold using DNA vs RNA HCR, yielding high signal-to-background ratios for both methods, with ~ 2 -fold improvement using DNA vs RNA HCR. Note that as autofluorescence increases (*i.e.*, as the imaging environment becomes increasingly challenging), the improvement in signal-to-background will approach the (~ 5 -fold) improvement in signal.

Comparing Signal Strength Using Direct-Labeled DNA Probes without and with DNA HCR *In Situ* Amplification. To estimate the signal gain per HCR amplification polymer, we compared the signal produced by direct-labeled DNA probes (each DNA probe carrying one fluorophore, no *in situ* amplification) to the amplified signal produced using DNA HCR (same direct-labeled probes, each HCR hairpin carrying one fluorophore). The signal generated using a single direct-labeled probe could not be distinguished from background, so these comparisons were performed using a probe set containing five probes. Using DNA HCR *in situ* amplification, the mean signal is ~ 200 -fold higher than using direct-labeled

probes without *in situ* amplification (Figure 5), consistent with a mean HCR polymer length of ~ 200 hairpins *in situ*.

Further Increasing Signal Gain Using Multiple Initiators per Probe and Multiple Probes per Target. To increase the signal per target even further, one strategy is to append more than one HCR initiator to each probe. However, the use of relatively short probes is beneficial in minimizing background, promoting deep sample penetration, and reducing synthesis cost. Hence, it is undesirable to append a large number of initiators to each probe. Figure 6 compares the performance of one-initiator DNA probes (I1 or I2) to that of a two-initiator DNA probe carrying one initiator at each end (I1 + I2; depicted in Figure 1bc). The signal using a two-initiator DNA probe is approximately equal to the sum of the signal generated by the two one-initiator DNA probes. The signal-to-background increases ~ 1.5 -fold using a two-initiator DNA probe vs either one-initiator DNA probe.

A second strategy to increase the signal per target is to detect each target using multiple probes that address different subsequences along the mRNA.^{4,9,33}

Due to variable probe hybridization yields, use of multiple probes per target also increases the chances of generating a strong signal on the first try using a new probe set for a new target. On the other hand, the cost

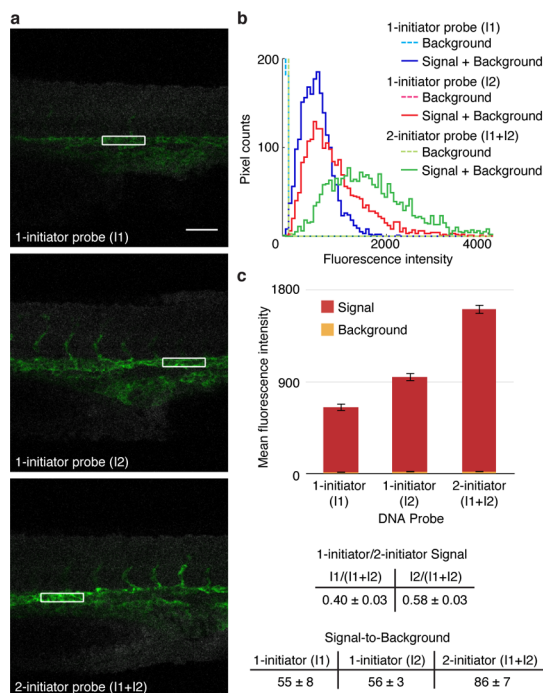


Figure 6. Comparing signal strength using DNA HCR *in situ* amplification with one-initiator and two-initiator DNA probes. (a) mRNA expression imaged by confocal microscopy with the microscope gain adjusted to avoid saturating pixels using the two-initiator DNA probe. Sample: whole-mount zebrafish embryo. Target: transgenic mRNA *Tg(flk1:egfp)*. Probe sets: one-initiator DNA probe (I1 or I2) or two-initiator DNA probe (I1 + I2). Green channel (excitation 633 nm): HCR-Alexa647 staining plus autofluorescence. Gray channel (excitation 488 nm): autofluorescence to depict sample morphology. Embryos fixed: 27 hpf. Scale bar: 50 μm . (b) Pixel intensity histograms for background (in WT embryos lacking the target; depicted rectangles in Figures S20–S22 in the SI) and signal plus background (in transgenic embryos containing the target; depicted rectangles in panel (a)). (c) Characterizing signal and background contributions for representative rectangles (mean \pm standard deviation, $N = 3$ embryos). See Section S4.3 in the SI for additional data.

of a probe set scales with its size so it is desirable to avoid using overly large probe sets. When mapping the expression pattern for a new target mRNA, we typically balance brightness, robustness, and cost considerations by using a probe set containing five two-initiator DNA probes (depicted in Figure 1c). If the signal is too low, we increase the number of probes in the probe set. If the background arising from nonspecific detection is too high, we test probes individually to eliminate those that exhibit poor selectivity.

Opportunities for Further Enhancing Signal-to-Background.

For biological samples that have substantially higher autofluorescence than whole-mount zebrafish embryos, it may prove necessary to produce even more signal per target molecule in order to achieve high signal-to-background. Potential approaches for further increasing signal-to-background include use of more than one fluorophore per HCR hairpin, use of more than two initiators per probe, and use of more than five probes per target molecule. In each case, it would be necessary to weigh the increase in signal against the corresponding increase in background (due to augmented nonspecific detection or nonspecific amplification), as well as any increases in the difficulty and cost of synthesis.

Multiplexed DNA HCR *in Situ* Amplification. Figure 7 demonstrates simultaneous mapping of four target mRNAs with high signal-to-background in a fixed whole-mount zebrafish embryo. Each target is detected using a probe set containing five two-initiator DNA probes; amplification is performed simultaneously for all targets using orthogonal DNA HCR amplifiers carrying spectrally distinct fluorophores.

Subcellular Signal Localization and Co-localization. Using HCR *in situ* amplification, each amplification polymer is expected to remain tethered to its initiating probe, suggesting the potential for subcellular signal localization and co-localization. To examine these properties, we double-detect a target mRNA using two independent probe sets each amplified using a spectrally distinct HCR amplifier; redundant detection of a single target mRNA provides a rigorous test of signal

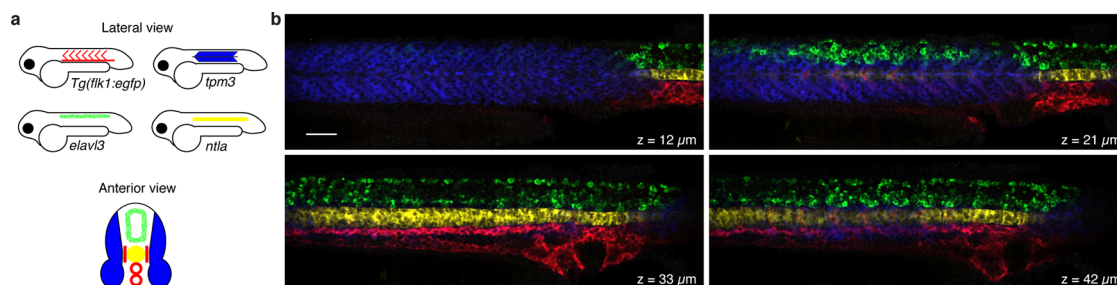


Figure 7. Multiplexed mapping of mRNA expression in a fixed whole-mount zebrafish embryo. (a) Expression atlas for four target mRNAs: *Tg(flk1:egfp)*, *tpm3*, *elavl3*, *ntlA*. (b) mRNA expression imaged via confocal microscopy at four planes within an embryo. Probe sets: five two-initiator DNA probes per target. Amplifiers: four orthogonal DNA HCR amplifiers carrying spectrally distinct fluorophores. Embryos fixed: 27 hpf. Scale bar: 50 μm . See Section S4.4 and Movie S1 in the SI for additional data.

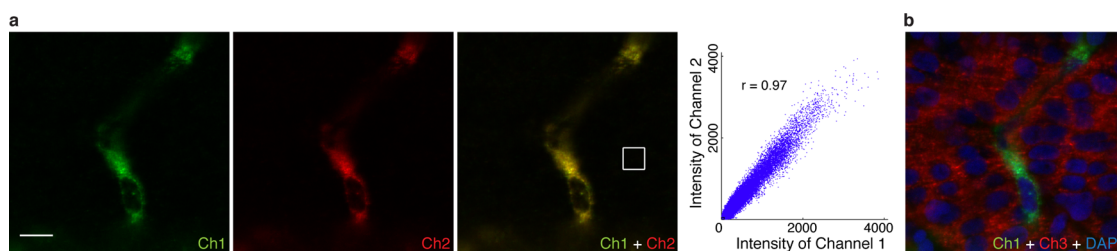


Figure 8. Subcellular signal localization and co-localization in a fixed whole-mount zebrafish embryo. Redundant two-color mapping of a target mRNA expressed predominantly in the interstices between somites (*Tg(flk1:egfp)*); two probe sets, two amplifiers, channels 1 and 2) simultaneous with mapping of a target mRNA expressed predominantly in the somites (*desm*; channel 3) and nuclear staining with DAPI. (a) Subcellular co-localization of *Tg(flk1:egfp)* signal (each pixel is 129 nm \times 129 nm) with highly correlated pixel intensities (Pearson correlation coefficient: $r = 0.97$). To avoid inflating the correlation coefficient, we exclude pixels that fall below background thresholds in both channels (excluded pixels fall in the black box at the lower left corner of the correlation plot). For each channel, the background threshold is defined as the mean plus two standard deviations for the pixels in the depicted white square. (b) Localization of signal within the cell cytoplasm for targets with interleaved expression patterns. Probe sets: three and five two-initiator DNA probes for *Tg(flk1:egfp)*, three two-initiator DNA probes for *desm*. Amplifiers: three orthogonal DNA HCR amplifiers carrying spectrally distinct fluorophores. Embryos fixed: 27 hpf. Scale bar: 10 μ m. See Section S4.5 in the SI for additional data.

co-localization independent of the expression pattern of the target. Figure 8a reveals subcellular co-localization of the signal (129 nm \times 129 nm pixels) and highly correlated pixel intensities (Pearson correlation coefficient: 0.97). To provide morphological context, Figure 8b includes nuclear staining with DAPI and HCR mapping of a second target mRNA predominantly expressed in the somites, revealing that the signal for both targets is localized in the cytoplasm and that the interstice between somites is the width of a single stretched cell. This study suggests that HCR polymers remain tethered to their initiating probes and demonstrates subcellular signal localization and co-localization within whole-mount zebrafish embryos.

CONCLUSIONS

This next-generation DNA HCR *in situ* amplification technology combines multiple improvements to dramatically increase the signal generated per target molecule, while simultaneously reducing reagent cost and increasing reagent durability. We identified permissive hybridization conditions (0% formamide, room temperature) suitable for DNA HCR *in situ* amplification, achieving low background without reducing the energetic driving force for HCR polymerization. To capitalize on this development, we engineered new

high-gain DNA HCR amplifiers for use in permissive hybridization conditions. To assist with future engineering efforts, we provide HCR design rules for dimensioning hairpins for prescribed experimental conditions. Because HCR is programmable, it is straightforward to engineer orthogonal amplifiers that operate independently for multiplexed studies. Within whole-mount zebrafish embryos, DNA HCR amplification polymers yield a \sim 200-fold increase in signal relative to use of direct-labeled DNA probes. Signal is further increased by detecting each target mRNA using a probe set containing five two-initiator DNA probes. Subcellular signal localization and co-localization are achieved, consistent with the expectation that HCR amplification polymers remain tethered to their initiating probes. Using orthogonal HCR amplifiers carrying spectrally distinct fluorophores, the time required to perform a multichannel experiment is no greater than for a one-channel experiment. Because the initiator sequences are independent of the target mRNAs, the amplifiers validated in the present work may be used without modification for future studies. The performance demonstrated here within intact zebrafish embryos suggests the suitability of next-generation DNA HCR amplifiers for use in diverse imaging settings as well as for diverse applications *in vitro*.

MATERIALS AND METHODS

Probe Synthesis. RNA probes are 81 nt long (26-nt initiator, 5-nt spacer, 50-nt mRNA recognition sequence). DNA one-initiator probes are 91 nt long (36-nt initiator, 5-nt spacer, 50-nt mRNA recognition sequence) and DNA two-initiator probes are 132 nt long with the second spacer and initiator downstream of the mRNA recognition sequence. mRNAs are addressed by probe sets containing one or more probes that hybridize at 50-nt binding sites. Probes were designed to minimize off-target complementarity using NCBI's BLAST *Danio rerio* RefSeq RNA database. Probe sequences are displayed in Section S5. RNA probes were synthesized by Molecular Instruments (www.molecularinstruments.org). DNA probes were

ordered as Ultramer oligonucleotides (unpurified) from Integrated DNA Technologies (IDT). Strands were resuspended in ultrapure water (resistance of 18 M Ω cm), and concentrations were determined by measuring absorption at 260 nm.

HCR Hairpin Design. RNA HCR hairpins are 52 nt long (10-nt toehold, 16-bp stem, 10-nt loop).³³ DNA HCR hairpins are 72 nt long (12-nt toehold, 24-bp stem, 12-nt loop). Hairpin dimensioning was performed based on *in vitro* and *in situ* studies performed in 5 \times SSC with 0.1% Tween 20. Sequences were designed using the multistate sequence design feature of the NUPACK web application,⁷² using target secondary structures for I1, H1, H2, I1 \cdot H1, and I1 \cdot H1 \cdot H2, as depicted in Figure 1a. HCR amplifier sequences are shown in Section S6.

HCR Hairpin Synthesis. RNA HCR hairpins were ordered from Molecular Instruments. DNA HCR hairpins were synthesized by IDT as standard DNA oligonucleotides end-labeled with an amine (3'-end for H1 and 5'-end for H2) to permit subsequent coupling to a fluorophore. The dye coupling reaction was performed by mixing an amine-labeled hairpin with an Alexa Fluor succinimidyl ester (Invitrogen) dissolved in DMF and incubating in the dark overnight. Alexa-labeled hairpins were separated from unincorporated dyes by using a 15% denaturing polyacrylamide gel. The bands corresponding to the expected sizes of the labeled hairpins were visualized by UV shadowing and excised from the gel. The DNA strands were then eluted by soaking in 0.3 M NaCl overnight and recovered by ethanol precipitation. The pellet was dried and resuspended in ultrapure water and quantified by measuring absorbance at 260 nm. To ensure that H1 and H2 form hairpin monomers, the strands were snap-cooled in 1× TE with 150 mM NaCl (RNA) or 5× SSC (DNA) before use (heat at 95 °C for 90 s, cool to room temperature on the benchtop for 30 min).

Gel Electrophoresis. RNA HCR reactions for Figure 2a were performed in 40% hybridization buffer without blocking agents (40% formamide, 2× SSC, 9 mM citric acid (pH 6.0), 0.1% Tween 20), and DNA HCR reactions for Figure 2b were performed in 5× SSC with 0.1% Tween 20. For 1.5 h reactions with each hairpin at 200 nM, RNA hairpins were snap-cooled separately at 3 μM in 1× TE with 150 mM NaCl, and DNA hairpins were snap-cooled separately at 3 μM in 5× SSC. The RNA and DNA initiators were diluted to three concentrations (3, 0.3, and 0.03 μM) in ultrapure water. In the RNA HCR gel, each lane was prepared by mixing 6 μL of formamide, 3 μL of 5× hybridization buffer supplements without blocking agents (10× SSC, 45 mM citric acid (pH 6.0), 0.5% Tween 20), 3 μL of ultrapure water, and 1 μL of each hairpin. In the DNA HCR gel, each lane was prepared by mixing 10 μL of 5× SSC, 1.5 μL of 10× SSC with 1% Tween 20, 0.5 μL of ultrapure water, and 1 μL of each hairpin. When an initiator was absent (lane 1), 1 μL of ultrapure water was added to bring the reaction volume to 15 μL. For the lanes with initiator at different dilutions (lanes 2–4), 1 μL of initiator was added. The reactions were incubated at 45 °C (RNA HCR) or room temperature (DNA HCR) for 1.5 h. The samples were supplemented with 3.75 μL of 5× gel loading buffer (50% glycerol with bromophenol blue and xylene cyanol tracking dyes) and loaded into a native 2% agarose gel, prepared with 1× LB buffer (Faster Better Media). The gel was run at 100 V for 100 min at room temperature and imaged using an FLA-5100 fluorescent scanner (Fujifilm Life Science) with a 635 nm laser and a 665 nm long-pass filter. The 1 kb DNA ladder (red) was prestained with SYBR Gold (Invitrogen) and imaged using a 488 nm laser and a 575 nm long-pass filter. For overnight reactions with each hairpin at 1 μM, reactions were performed analogously. In this case, the RNA hairpins were snap-cooled separately at 7.5 μM in 1× TE with 150 mM NaCl in order to maintain the 15 μL reaction volume. Gel electrophoresis was performed as for the 1.5 h reactions.

DNA multiplexed reactions for Figure 3 were performed in 5× SSC with 0.1% Tween 20. Each of the eight hairpin species (two for each of the four HCR amplifiers) was snap-cooled at 4 μM in 5× SSC. The DNA initiator for each HCR system was diluted to 0.1 μM in ultrapure water. Each lane was prepared by mixing 2.5 μL of 10× SSC with 1% Tween 20, 1.5 μL of ultrapure water, and 2.5 μL of each of the eight hairpins. When an initiator was absent (lane 1), 1 μL of ultrapure water was added to bring the reaction volume to 25 μL. For lanes 2 to 5, 1 μL of 0.1 μM initiator for one HCR amplifier was added. The reactions were incubated at room temperature for 4 h. The samples were supplemented with 6.25 μL of 5× gel loading buffer and loaded into a native 2% agarose gel. The gel was run at 100 V for 90 min at room temperature and imaged using an FLA-5100 fluorescent scanner. The excitation laser sources and emission filters were as follows: 473 nm laser with 530 ± 10 nm bandpass filter (amplifier B2, Alexa 488), 532 nm laser with 570 ± 10 nm bandpass filter (amplifier B1, Alexa 546), 635 nm laser with 665 nm long-pass filter (amplifier B4, Alexa 647), and 670 nm laser with 705 nm long-pass filter (amplifier B3, Alexa 700).

In Situ Hybridization. Procedures for the care and use of zebrafish embryos were approved by the Caltech IACUC. Embryos were fixed and permeabilized using the protocol

of Section S1.1. Transgenic embryos expressing target mRNA, *Tg(flk1:egfp)*, were identified based on GFP fluorescence using a Leica MZ16 FA fluorescence stereomicroscope. *In situ* hybridization experiments were performed using the protocols of Sections S1.3 (RNA HCR) and S1.5 (DNA HCR). Overnight incubations were performed for 16 h. For the direct-labeled DNA probe experiments of Figure 5, the DNA HCR protocol was used with HCR hairpins omitted from the amplification stage.

Confocal Microscopy. A chamber for mounting the embryo was made by aligning two stacks of Scotch tape (8 pieces per stack) 1 cm apart on a 25 mm × 75 mm glass slide (VWR). Approximately 200 μL of 3% methyl cellulose mounting medium was added between the tape stacks on the slide, and embryos were placed on the medium oriented for lateral imaging. A 22 mm × 22 mm No. 1 coverslip (VWR) was placed on top of the stacks to close the chamber. A Zeiss 710 NLO inverted confocal microscope was used to acquire all images, using either an LD LCI Plan-Apochromat 25×/0.8 Imm Corr DIC objective (Figures 4–7) or an LD C-Apochromat 40×/1.1 W Corr objective (Figure 8). For Figures 4–6, excitation laser sources and tuned emissions bandpass filters were 488 nm/501–552 nm (gray; autofluorescence) and 633 nm/639–758 nm (green; Alexa 647). For Figure 7, excitation laser sources and tuned emission bandpass filters were 488 nm/489–519 nm (Alexa 488), 514 nm/550–565 nm (Alexa 514), 561 nm/563–621 nm (Alexa 546), and 633 nm/660–758 nm (Alexa 647). For Figure 8, embryos were incubated in SlowFade Gold Antifade Reagent with DAPI (Molecular Probes) for 30 min before mounting. Excitation laser sources and tuned emission bandpass filters were 488 nm/491–515 nm (Alexa 488), 514 nm/550–565 nm (Alexa 514), 561 nm/574–613 nm (Alexa 546), and 800 nm (two-photon laser)/410–557 nm (DAPI). All images are presented without background subtraction.

Image Analysis. Using the *in situ* protocol, background (BACK) is characterized for pixels in a region of nonexpression, and the combination of background and signal (BACK+SIG) is characterized for pixels in a region of high expression. For validation studies (Figures 4–6), we employ a transgenic target mRNA so that BACK pixel intensities may be obtained from a WT embryo lacking the target; BACK+SIG pixel intensities are obtained from a transgenic embryo containing the target. For each embryo, we analyze pixels in a representative rectangular region of a representative optical section. For the pixels in a given rectangle, we characterize the distribution by plotting a pixel intensity histogram (Figures 4b, 5b, 6b) and characterize typical performance by calculating the mean pixel intensity (\bar{x}_{BACK} or $\bar{x}_{\text{BACK+SIG}}$). Performance across embryos is characterized by calculating the sample means, \bar{x}_{BACK} and $\bar{x}_{\text{BACK+SIG}}$, and sample standard deviations, s_{BACK} and $s_{\text{BACK+SIG}}$ ($N = 3$ rectangles for each type of experiment, one per embryo). The mean signal is then estimated as

$$\bar{x}_{\text{SIG}} = \bar{x}_{\text{BACK+SIG}} - \bar{x}_{\text{BACK}}$$

with standard deviation estimated *via* uncertainty propagation as

$$s_{\text{SIG}} \leq \sqrt{(s_{\text{BACK+SIG}})^2 + (s_{\text{BACK}})^2}$$

as displayed in the bar graphs of Figures 4c, 5c, and 6c. The signal-to-background ratio is estimated as

$$\bar{x}_{\text{SIG/BACK}} = \bar{x}_{\text{SIG}}/\bar{x}_{\text{BACK}}$$

with standard deviation estimated *via* uncertainty propagation as

$$s_{\text{SIG/BACK}} \leq \frac{\bar{x}_{\text{SIG}}}{\bar{x}_{\text{BACK}}} \sqrt{\left(\frac{s_{\text{SIG}}}{\bar{x}_{\text{SIG}}}\right)^2 + \left(\frac{s_{\text{BACK}}}{\bar{x}_{\text{BACK}}}\right)^2}$$

The signal-to-signal ratio for the two methods is calculated analogously. These upper bounds on estimated standard deviations hold under the assumption that the correlation between SIG and BACK is non-negative.

Conflict of Interest: The authors declare the following competing financial interest(s): Patents and pending patent applications.

Acknowledgment. We thank B. R. Wolfe, J. N. Zadeh, and R. M. Dirks for the use of unpublished multistate sequence design

software. We thank L. M. Hochrein, V. Trivedi, J. R. Viereg, B. R. Wolfe, and S. E. Fraser for helpful discussions and M. Kirk for assistance with bibliography preparation. This work draws on molecular architectures and sequence design algorithms developed within the NSF Molecular Programming Project (NSF-CCF-0832824 and NSF-CCF-1317694) and was funded by the NIH (5R01EB006192), the Gordon and Betty Moore Foundation (GBMF2809), and the Beckman Institute at Caltech (Programmable Molecular Technology Center).

Supporting Information Available: *In situ* hybridization protocols, nonspecific hairpin binding studies, *in silico* and *in vitro* analysis of DNA HCR amplifiers, characterization of background and signal *in situ*, probe sequences, and HCR amplifier sequences. This material is available free of charge via the Internet at <http://pubs.acs.org>.

REFERENCES AND NOTES

- Qian, X.; Jin, L.; Lloyd, R. V. *In Situ* Hybridization: Basic Approaches and Recent Development. *J. Histotechnol.* **2004**, *27*, 53–67.
- Silverman, A.; Kool, E. Oligonucleotide Probes for RNA-Targeted Fluorescence *In Situ* Hybridization. *Adv. Clin. Chem.* **2007**, *43*, 79–115.
- Kislauskis, E. H.; Li, Z.; Singer, R. H.; Taneja, K. L. Isoform-Specific 3'-Untranslated Sequences Sort α -Cardiac and β -Cytoplasmic Actin Messenger RNAs to Different Cytoplasmic Compartments. *J. Cell Biol.* **1993**, *123*, 165–172.
- Femino, A.; Fay, F. S.; Fogarty, K.; Singer, R. H. Visualization of Single RNA Transcripts *In Situ*. *Science* **1998**, *280*, 585–590.
- Levsky, J. M.; Shenoy, S. M.; Pezo, R. C.; Singer, R. H. Single-Cell Gene Expression Profiling. *Science* **2002**, *297*, 836–840.
- Kosman, D.; Mizutani, C. M.; Lemons, D.; Cox, W. G.; McGinnis, W.; Bier, E. Multiplex Detection of RNA Expression in *Drosophila* Embryos. *Science* **2004**, *305*, 846.
- Capodiceci, P.; Donovan, M.; Buchinsky, H.; Jeffers, Y.; Cordon-Cardo, C.; Gerald, W.; Edelson, J.; Shenoy, S. M.; Singer, R. H. Gene Expression Profiling in Single Cells within Tissue. *Nat. Methods* **2005**, *2*, 663–665.
- Chan, P. M.; Yuen, T.; Ruf, F.; Gonzalez-Maeso, J.; Sealfon, S. C. Method for Multiplex Cellular Detection of mRNAs Using Quantum Dot Fluorescent *In Situ* Hybridization. *Nucleic Acids Res.* **2005**, *33*, e161.
- Raj, A.; van den Bogaard, P.; Rifkin, S. A.; van Oudenaarden, A.; Tyagi, S. Imaging Individual mRNA Molecules Using Multiple Singly Labeled Probes. *Nat. Methods* **2008**, *5*, 877–879.
- Macechko, P. T.; Krueger, L.; Hirsch, B.; Erlandsen, S. L. Comparison of Immunological Amplification versus Enzymatic Deposition of Fluorochrome-Conjugated Tyramide as Detection Systems for FISH. *J. Histochem. Cytochem.* **1997**, *45*, 359–363.
- Collins, M. L.; Irvine, B.; Tyner, D.; Fine, E.; Zayati, C.; Chang, C. A.; Horn, T.; Ahle, D.; Detmer, J.; Shen, L.-P.; Kolberg, J.; Bushnell, S.; Urdea, M. S.; Ho, D. D. A Branched DNA Signal Amplification Assay for Quantification of Nucleic Acid Targets below 100 Molecules/ml. *Nucleic Acids Res.* **1997**, *25*, 2979–2984.
- Hughes, S. C.; Krause, H. M. Double Labeling with Fluorescence *In Situ* Hybridization in *Drosophila* Whole-Mount Embryos. *BioTechniques* **1998**, *24*, 530–532.
- Bushnell, S.; Budde, J.; Catino, T.; Cole, J.; Derti, A.; Kelso, R.; Collins, M. L.; Molino, G.; Sheridan, P.; Monahan, J.; Urdea, M. ProbeDesigner: For the Design of Probesets for Branched DNA (bDNA) Signal Amplification Assays. *Bioinformatics* **1999**, *15*, 348–355.
- Wiedorn, K. H.; Kuhl, H.; Galle, J.; Caselitz, J.; Vollmer, E. Comparison of *In-Situ* Hybridization, Direct and Indirect *In-Situ* PCR as Well as Tyramide Signal Amplification for the Detection of HPV. *Histochem. Cell Biol.* **1999**, *111*, 89–95.
- Player, A. N.; Shen, L. P.; Kenny, D.; Antao, V. P.; Kolberg, J. A. Single-Copy Gene Detection Using Branched DNA (bDNA) *In Situ* Hybridization. *J. Histochem. Cytochem.* **2001**, *49*, 603–611.
- Zhou, Y.; Calciano, M.; Hamann, S.; Leamon, J. H.; Strugnell, T.; Christian, M. W.; Lizardi, P. M. *In Situ* Detection of Messenger RNA Using Digoxigenin-Labeled Oligonucleotides and Rolling Circle Amplification. *Exp. Mol. Pathol.* **2001**, *70*, 281–288.
- Schweitzer, B.; Kingsmore, S. Combining Nucleic Acid Amplification and Detection. *Curr. Opin. Biotechnol.* **2001**, *12*, 21–27.
- Qian, X.; Lloyd, R. V. Recent Developments in Signal Amplification Methods for *In Situ* Hybridization. *Diagn. Mol. Pathol.* **2003**, *12*, 1–13.
- Larsson, C.; Koch, J.; Nygren, A.; Janssen, G.; Raap, A. K.; Landegren, U.; Nilsson, M. *In Situ* Genotyping Individual DNA Molecules by Target-Primed Rolling-Circle Amplification of Padlock Probes. *Nat. Methods* **2004**, *1*, 227–232.
- Zhou, H.; Bouwman, K.; Schotanus, M.; Verweij, C.; Marrero, J. A.; Dillon, D.; Costa, J.; Lizardi, P.; Haab, B. B. Two-Color, Rolling-Circle Amplification on Antibody Microarrays for Sensitive, Multiplexed Serum-Protein Measurements. *Genome Biol.* **2004**, *5*, R28.
- Larsson, C.; Grundberg, I.; Soderberg, O.; Nilsson, M. *In Situ* Detection and Genotyping of Individual mRNA Molecules. *Nat. Methods* **2010**, *7*, 395–397.
- Harland, R. M. *In Situ* Hybridization: An Improved Whole-Mount Method for *Xenopus* Embryos. *Methods Cell Biol.* **1991**, *36*, 685–695.
- Speel, E. J. M.; Hopman, A. H. N.; Komminoth, P. Amplification Methods to Increase the Sensitivity of *In Situ* Hybridization: Play CARD(S). *J. Histochem. Cytochem.* **1999**, *47*, 281–288.
- Denkers, N.; Garcia-Villalba, P.; Rodesch, C. K.; Nielson, K. R.; Mauch, T. J. FISHing for Chick Genes: Triple-Label Whole-Mount Fluorescence *In Situ* Hybridization Detects Simultaneous and Overlapping Gene Expression in Avian Embryos. *Dev. Dyn.* **2004**, *229*, 651–657.
- Barroso-Chinea, P.; Aymerich, M. S.; Castle, M. M.; Perez-Manso, M.; Tunon, T.; Erro, E.; Lanciego, J. L. Detection of Two Different mRNAs in a Single Section by Dual *In Situ* Hybridization: A Comparison between Colorimetric and Fluorescent Detection. *J. Neurosci. Methods* **2007**, *162*, 119–128.
- van Gijlswijk, R. P. M.; Wiegant, J.; Raap, A. K.; Tanke, H. J. Improved Localization of Fluorescent Tyramides for Fluorescence *In Situ* Hybridization Using Dextran Sulfate and Polyvinyl Alcohol. *J. Histochem. Cytochem.* **1996**, *44*, 389–392.
- Speel, E. J. M. Detection and Amplification Systems for Sensitive, Multiple-Target DNA and RNA *In Situ* Hybridization: Looking inside Cells with a Spectrum of Colors. *Histochem. Cell Biol.* **1999**, *112*, 89–113.
- Thisse, B.; Heyer, V.; Lux, A.; Alunni, V.; Degrave, A.; Seiliez, I.; Kirchner, J.; Parkhill, J. P.; Thisse, C. Spatial and Temporal Expression of the Zebrafish Genome by Large-Scale *In Situ* Hybridization Screening. In *The Zebrafish: 2nd ed.; Genetics Genomics and Informatics*; Detrich, H. W. D., III; Zon, L. I., Westerfield, M., Eds.; Elsevier Academic Press: San Diego, CA, 2004; pp 505–519.
- Acloque, H.; Wilkinson, D. G.; Nieto, M. A. *In Situ* Hybridization Analysis of Chick Embryos in Whole-Mount and Tissue Sections. In *Avian Embryology*, 2nd ed.; Bronner-Fraser, M., Ed.; Elsevier Academic Press: San Diego, CA, 2008; pp 169–185.
- Zhang, D. Y.; Seelig, G. Dynamic DNA Nanotechnology Using Strand-Displacement Reactions. *Nat. Chem.* **2011**, *3*, 103–113.
- Gall, J. G.; Pardue, M. L. Formation and Detection of RNA-DNA Hybrid Molecules in Cytological Preparations. *Proc. Natl. Acad. Sci. U.S.A.* **1969**, *63*, 378–383.
- Dirks, R. M.; Pierce, N. A. Triggered Amplification by Hybridization Chain Reaction. *Proc. Natl. Acad. Sci. U.S.A.* **2004**, *101*, 15275–15278.
- Choi, H. M. T.; Chang, J.; Trinh, L. A.; Padilla, J.; Fraser, S. E.; Pierce, N. A. Programmable *In Situ* Amplification for Multiplexed Imaging of mRNA Expression. *Nat. Biotechnol.* **2010**, *28*, 1208–1212.
- Shimron, S.; Wang, F.; Orbach, R.; Willner, I. Amplified Detection of DNA through the Enzyme-Free Autonomous Assembly of Hemin/G-Quadruplex DNAAzyme Nanowires. *Anal. Chem.* **2012**, *84*, 1042–1048.
- Tang, W.; Wang, D.; Xu, Y.; Li, N.; Liu, F. A Self-Assembled DNA Nanostructure-Amplified Quartz Crystal Microbalance

- with Dissipation Biosensing Platform for Nucleic Acids. *Chem. Commun.* **2012**, *48*, 6678–6680.
36. Zhao, J.; Chen, C.; Zhang, L.; Jiang, J.; Yu, R. An Electrochemical Aptasensor based on Hybridization Chain Reaction with Enzyme-Signal Amplification for Interferon-Gamma Detection. *Biosens. Bioelectron.* **2012**, *36*, 129–134.
 37. Chen, Y.; Xu, J.; Su, J.; Xiang, Y.; Yuan, R.; Chai, Y. *In Situ* Hybridization Chain Reaction Amplification for Universal and Highly Sensitive Electrochemiluminescent Detection of DNA. *Anal. Chem.* **2012**, *84*, 7750–7755.
 38. Zhuang, J.; Fu, L.; Xu, M.; Yang, H.; Chen, G.; Tang, D. Sensitive Electrochemical Monitoring of Nucleic Acids Coupling DNA Nanostructures with Hybridization Chain Reaction. *Anal. Chim. Acta* **2013**, *783*, 17–23.
 39. Wang, X.; Lau, C.; Kai, M.; Lu, J. Hybridization Chain Reaction-Based Instantaneous Derivatization Technology for Chemiluminescence Detection of Specific DNA Sequences. *Analyst* **2013**, *138*, 2691–2697.
 40. Wang, C.; Zhou, H.; Zhu, W.; Li, H.; Jiang, J.; Shen, G.; Yu, R. Ultrasensitive Electrochemical DNA Detection Based on Dual Amplification of Circular Strand-Displacement Polymerase Reaction and Hybridization Chain Reaction. *Biosens. Bioelectron.* **2013**, *47*, 324–328.
 41. Liu, S. F.; Wang, Y.; Ming, J. J.; Lin, Y.; Cheng, C. B.; Li, F. Enzyme-Free and Ultrasensitive Electrochemical Detection of Nucleic Acids by Target Catalyzed Hairpin Assembly Followed with Hybridization Chain Reaction. *Biosens. Bioelectron.* **2013**, *49*, 472–477.
 42. Song, W.; Zhu, K.; Cao, Z.; Lau, C.; Lu, J. Hybridization Chain Reaction-Based Aptameric System for the Highly Selective and Sensitive Detection of Protein. *Analyst* **2012**, *137*, 1396–1401.
 43. Zhu, G. Z.; Zhang, S. F.; Song, E. Q.; Zheng, J.; Hu, R.; Fang, X. H.; Tan, W. H. Building Fluorescent DNA Nanodevices on Target Living Cell Surfaces. *Angew. Chem., Int. Ed.* **2013**, *52*, 5490–5496.
 44. Zhu, G. Z.; Zheng, J.; Song, E. Q.; Donovan, M.; Zhang, K. J.; Liu, C.; Tan, W. H. Self-Assembled, Aptamer-Tethered DNA Nanotrains for Targeted Transport of Molecular Drugs in Cancer Theranostics. *Proc. Natl. Acad. Sci. U.S.A.* **2013**, *110*, 7998–8003.
 45. Bai, L.; Chai, Y. Q.; Yuan, R.; Yuan, Y. L.; Xie, S. B.; Jiang, L. P. Amperometric Aptasensor for Thrombin Detection Using Enzyme-Mediated Direct Electrochemistry and DNA-Based Signal Amplification Strategy. *Biosens. Bioelectron.* **2013**, *50*, 325–330.
 46. Xu, Q. F.; Zhu, G. C.; Zhang, C. Y. Homogeneous Bioluminescence Detection of Biomolecules Using Target-Triggered Hybridization Chain Reaction-Mediated Ligation without Luciferase Label. *Anal. Chem.* **2013**, *85*, 6915–6921.
 47. Zhang, J.; Chai, Y. Q.; Yuan, R.; Yuan, Y. L.; Bai, L. J.; Xie, S. B.; Jiang, L. P. A Novel Electrochemical Aptasensor for Thrombin Detection Based on the Hybridization Chain Reaction with Hemin/G-Quadruplex DNAzyme-Signal Amplification. *Analyst* **2013**, *138*, 4558–4564.
 48. Choi, J.; Love, K. R.; Gong, Y.; Gierahn, T. M.; Love, J. C. Immuno-Hybridization Chain Reaction for Enhancing Detection of Individual Cytokine-Secreting Human Peripheral Mononuclear Cells. *Anal. Chem.* **2011**, *83*, 6890–6895.
 49. Zhou, J.; Xu, M.; Tang, D.; Gao, Z.; Tang, J.; Chen, G. Nanogold-Based Bio-Bar Codes for Label-Free Immunosensing of Proteins Coupling with an *In Situ* DNA-Based Hybridization Chain Reaction. *Chem. Commun.* **2012**, *48*, 12207–12209.
 50. Zhang, B.; Liu, B. Q.; Tang, D. P.; Niessner, R.; Chen, G. N.; Knopp, D. DNA-Based Hybridization Chain Reaction for Amplified Bioelectronic Signal and Ultrasensitive Detection of Proteins. *Anal. Chem.* **2012**, *84*, 5392–5399.
 51. Chen, N.; Li, S.; Battig, M. R.; Wang, Y. Programmable Imaging Amplification *via* Nanoparticle-Initiated DNA Polymerization. *Small* **2013**, *9*, 3944–3949.
 52. Xu, J.; Wu, J.; Zong, C.; Ju, H.; Yan, F. Manganese Porphyrin-DNA Complex: A Mimicking Enzyme for Highly Efficient Bioanalysis. *Anal. Chem.* **2013**, *85*, 3374–3379.
 53. Zhou, J.; Lai, W.; Zhuang, J.; Tang, J.; Tang, D. Nanogold-Functionalized DNAzyme Concatamers with Redox-Active Intercalators for Quadruple Signal Amplification of Electrochemical Immunoassay. *ACS Appl. Mater. Interfaces* **2013**, *5*, 2773–2781.
 54. Han, J.; Zhuo, Y.; Chai, Y. Q.; Yu, Y. Q.; Liao, N.; Yuan, R. Electrochemical Immunoassay for Thyroxine Detection Using Cascade Catalysis as Signal Amplified Enhancer and Multi-Functionalized Magnetic Graphene Sphere as Signal Tag. *Anal. Chim. Acta* **2013**, *790*, 24–30.
 55. Tong, L.; Wu, J.; Li, J.; Ju, H. X.; Yan, F. Hybridization Chain Reaction Engineered DNA Nanopolylinker for Amplified Electrochemical Sensing of Biomarkers. *Analyst* **2013**, *138*, 4870–4876.
 56. Zhuang, J.; Fu, L.; Xu, M.; Zhou, Q.; Chen, G.; Tang, D. DNAzyme-Based Magneto-Controlled Electronic Switch for Picomolar Detection of Lead (II) Coupling with DNA-Based Hybridization Chain Reaction. *Biosens. Bioelectron.* **2013**, *45*, 52–57.
 57. Chemeris, D. A.; Nikonorov, Y. M.; Vakhitov, V. A. Real-Time Hybridization Chain Reaction. *Dokl. Biochem. Biophys.* **2008**, *419*, 53–55.
 58. Niu, S. Y.; Jiang, Y.; Zhang, S. S. Fluorescence Detection for DNA Using Hybridization Chain Reaction with Enzyme-Amplification. *Chem. Commun.* **2010**, *46*, 3089–3091.
 59. Ren, J.; Wang, J.; Han, L.; Wang, E.; Wang, J. Kinetically Grafting G-Quadruplexes onto DNA Nanostructures for Structure and Function Encoding *via* a DNA Machine. *Chem. Commun.* **2011**, *47*, 10563–10565.
 60. Huang, J.; Wu, Y.; Chen, Y.; Zhu, Z.; Yang, X.; Yang, C. J.; Wang, K.; Tan, W. Pyrene-Excimer Probes Based on the Hybridization Chain Reaction for the Detection of Nucleic Acids in Complex Biological Fluids. *Angew. Chem., Int. Ed.* **2011**, *50*, 401–404.
 61. Wang, F.; Elbaz, J.; Orbach, R.; Magen, N.; Willner, I. Amplified Analysis of DNA by the Autonomous Assembly of Polymers Consisting of DNAzyme Wires. *J. Am. Chem. Soc.* **2011**, *133*, 17149–17151.
 62. Chen, R.; Dong, J.; Cui, X.; Wang, W.; Yasmeen, A.; Deng, Y.; Zeng, X.; Tang, Z. DNA Based Identification of Medicinal Materials in Chinese Patent Medicines. *Sci. Rep.* **2012**, *2*, 958.
 63. Dong, J.; Cui, X.; Deng, Y.; Tang, Z. Amplified Detection of Nucleic Acid by G-Quadruplex Based Hybridization Chain Reaction. *Biosens. Bioelectron.* **2012**, *38*, 258–263.
 64. Jiang, Y.; Li, B.; Chen, X.; Ellington, A. D. Coupling Two Different Nucleic Acid Circuits in an Enzyme-Free Amplifier. *Molecules* **2012**, *17*, 13211–13220.
 65. Wang, P.; Ge, Z. L.; Pei, H.; Wang, L. H.; Fan, C. H. Quartz Crystal Microbalance Studies on Surface-Initiated DNA Hybridization Chain Reaction. *Acta Chim. Sin.* **2012**, *70*, 2127–2132.
 66. Yang, L.; Liu, C. H.; Ren, W.; Li, Z. P. Graphene Surface-Anchored Fluorescence Sensor for Sensitive Detection of MicroRNA Coupled with Enzyme-Free Signal Amplification of Hybridization Chain Reaction. *ACS Appl. Mater. Interfaces* **2012**, *4*, 6450–6453.
 67. Ren, W.; Liu, H.; Yang, W.; Fan, Y.; Yang, L.; Wang, Y.; Liu, C.; Li, Z. A Cytometric Bead Assay for Sensitive DNA Detection Based on Enzyme-Free Signal Amplification of Hybridization Chain Reaction. *Biosens. Bioelectron.* **2013**, *49*, 380–386.
 68. Liu, P.; Yang, X. H.; Sun, S.; Wang, Q.; Wang, K. M.; Huang, J.; Liu, J. B.; He, L. L. Enzyme-Free Colorimetric Detection of DNA by Using Gold Nanoparticles and Hybridization Chain Reaction Amplification. *Anal. Chem.* **2013**, *85*, 7689–7695.
 69. Quartin, R. S.; Plewiska, M.; Wetmur, J. G. Branch Migration Mediated DNA Labeling and Cloning. *Biochemistry* **1989**, *28*, 8676–8682.
 70. Yurke, B.; Turberfield, A. J.; Mills, A. P., Jr.; Simmel, F. C.; Neumann, J. L. A DNA-Fuelled Molecular Machine Made of DNA. *Nature* **2000**, *406*, 605–608.

71. Choi, H. M. T. *Programmable in Situ Amplification for Multiplexed Bioimaging*. Ph.D. Thesis, California Institute of Technology, 2009.
72. Zadeh, J. N.; Steenberg, C. D.; Bois, J. S.; Wolfe, B. R.; Pierce, M. B.; Khan, A. R.; Dirks, R. M.; Pierce, N. A. NUPACK: Analysis and Design of Nucleic Acid Systems. *J. Comput. Chem.* **2011**, *32*, 170–173.
73. Zadeh, J. N.; Wolfe, B. R.; Pierce, N. A. Nucleic Acid Sequence Design via Efficient Ensemble Defect Optimization. *J. Comput. Chem.* **2011**, *32*, 439–452.
74. Dirks, R. M.; Lin, M.; Winfree, E.; Pierce, N. A. Paradigms for Computational Nucleic Acid Design. *Nucleic Acids Res.* **2004**, *32*, 1392–1403.
75. Dirks, R. M.; Bois, J. S.; Schaeffer, J. M.; Winfree, E.; Pierce, N. A. Thermodynamic Analysis of Interacting Nucleic Acid Strands. *SIAM Rev.* **2007**, *49*, 65–88.